Solar Energy 173 (2018) 955–963

Contents lists available at ScienceDirect

Solar Energy

journal homepage: www.elsevier.com/locate/solener

$Cu_2ZnSnSe_4$ based solar cells combining co-electrodeposition and rapid thermal processing

M. Valdés[a,b,*], A. Hernández-Martinez[b], Y. Sánchez[b], F. Oliva[b], V. Izquierdo-Roca[b], A. Perez Rodriguez[b,c], E. Saucedo[b]

[a] Electroquímica Aplicada, INTEMA, Facultad de Ingeniería, CONICET-Universidad Nacional de Mar del Plata, Av. Colón 10500, 7600 Mar del Plata, Argentina
[b] Catalonia Institute for Energy Research (IREC), Jardins de les Dones de Negre 1, 08930 Sant Adrià del Besòs-Barcelona, Spain
[c] IN2UB, Departament d' Electrònica, Universitat de Barcelona, C. Martí i Franquès 1, 08028 Barcelona, Spain

ARTICLE INFO

Keywords:
Co-electrodeposition
Precursor
Rapid thermal processing
Kesterite
Solar cells

ABSTRACT

In this work, a fast two-step process combining co-electrodeposition of a CuZnSn precursor plus a reactive selenization step with a rapid thermal annealing to synthesize $Cu_2ZnSnSe_4$ thin films is presented. By tuning the electrochemical procedure is feasible to obtain with a short electrodeposition time (15 min) the precursor composition required for high efficiency solar cell devices. XRD characterization reveals that the precursor is mainly composed of binary Cu-Zn and Cu-Sn alloys that after thermal treatment completely react to form a kesterite thin film. Raman spectra and Raman mappings demonstrate that best quality kesterite films are obtained after selective chemical etching necessary to remove secondary phases, like ZnSe and SnSe, which are detrimental for solar cell performance. Best solar cells prototypes achieve efficiencies of 5% with a current density of 30.9 mA/cm^2, an open circuit potential of 327 mV and a fill factor of 51.5%. The low value of open circuit voltage is attributed to the presence of voids and partial delamination observed in the Mo/$Cu_2ZnSnSe_4$ interface.

1. Introduction

In the last decade, kesterite ($Cu_2ZnSnSe_4$ or CZTSe) has emerged as an excellent thin film absorber for photovoltaic devices. This material has excellent optical properties ($\alpha \geq 10^4\ cm^{-1}$ in the visible range) and a direct band gap energy value (E_{GAP}) that matches the solar spectrum ($E_{GAP} \sim 1$ eV) (Platzer-Björkman, 2017; Siebentritt, 2017). As opposed to Cu(In,Ga)Se_2 (CIGSe) technology, kesterite is more attractive due the earth abundance of its constituent elements which, from an industrial point of view, is a key aspect to ensure mass production compatible with several GW of production in the medium and long term (Almosni et al., 2018; Wallace et al., 2017). A world-record 12.6% power conversion efficiency has been achieved using a mixed CZTSSe absorber composition (Wang et al., 2014).

CZTSe films are usually obtained by "two-steps" or sequential processes, consisting on the deposition of a precursor, either composed by metallic stacks (Cu/Zn/Sn) or by metal-chalcogenides, followed by a reactive annealing in selenium containing atmosphere. Using sequential approaches, a record efficiency of 11.8% has been reported for a CZTSe solar cell, using an innovative approach based on the introduction of very small Ge quantities (Giraldo et al., 2018).

In order to achieve real cost reductions and competitiveness, this sequential processes requires the development of cost-efficient methodologies. First, the precursor must be obtained with a low-cost technique that can be easily transferable to industrial scale. Electrodeposition meets this requirement and has been used for decades in coatings with applications in several fields (Djokić, 2014; Popov et al., 2016). Besides, electrolytes are prepared from low-cost and eco-friendly aqueous solution in contrast to other chemical routes that use highly toxic and more expensive solvent such as hydrazine (Wang et al., 2014). There are several electrodeposition routes that can be used to obtain a precursor that after a selenization/sulfurization treatment is converted into CZTSe or CZTS films. Detailed information on each of these routes can be found in reviewing article of Colombara et al. (2015). Record efficiencies of 8.2% for a pure selenide $Cu_2ZnSnSe_4$ (CZTSe) device (Vauche et al., 2016) and 8% for a pure-sulfide CZTS device (Jiang et al., 2014) were reported using electrodeposition. In these works, the electrodeposition of stacked layers of individual elements, also known as the SEL route, has been used to deposit a precursor material, followed by a treatment in Se or S atmosphere to

* Corresponding author at: Electroquímica Aplicada, INTEMA, Facultad de Ingeniería, CONICET-Universidad Nacional de Mar del Plata, Av. Colón 10500, 7600 Mar del Plata, Argentina.
E-mail address: mvaldes@fi.mdp.edu.ar (M. Valdés).

https://doi.org/10.1016/j.solener.2018.08.049
Received 7 June 2018; Received in revised form 6 August 2018; Accepted 19 August 2018
0038-092X/ © 2018 Elsevier Ltd. All rights reserved.

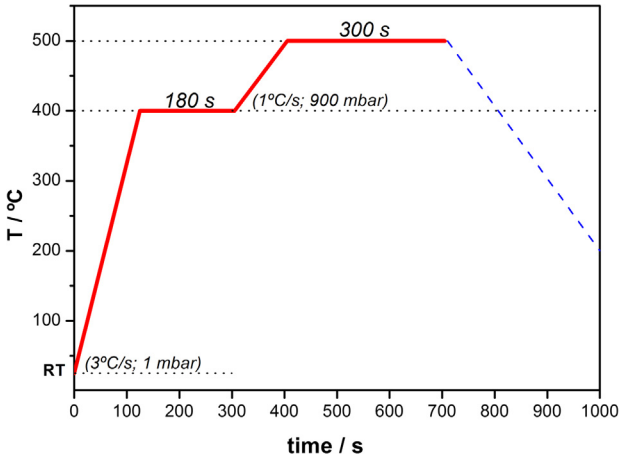

Fig. 1. Temperature – time profile used during RTP for selenization of CZT precursors. Heating rate and argon background pressure are indicated in brackets at each stage.

transform the precursor into a high quality CZTSe or CZTS film. Another route is based on the co-electrodeposition of a metallic CuZnSn precursor. In contrast to the SEL route where three separate electrolytes and three electrochemical steps are needed to obtain the metallic stack, this method is highly attractive because it involves a single electrolyte and one-electrodeposition step to form a precursor film. Despite this, certain disadvantages related to inhomogeneous deposition and problems with bath stability explain why co-electrodeposited kesterite devices have presented lower efficiencies than those prepared with the SEL route, in addition to the difficulties to accurately control the precursor metallic composition. Efficiencies in the range 2–6% are found in literature for the co-electrodeposition route followed by a selenization or sulfurization treatment (Gougaud et al., 2013; Khalil et al., 2017; Kim et al., 2015; Kondrotas et al., 2015; Li et al., 2014; Rakhshani et al., 2017; Zhang et al., 2013), but most reported efficiencies were only achieved when a low-temperature thermal treatment of the CZT precursor is carried out prior the Se or S annealing. A remarkable pure selenide (CZTSe) 8.0% power conversion efficiency has been achieved with a layer obtained by a single selenization of a co-electrodeposited CZT metallic precursor (Jeon et al., 2014), while 7.4% PCE solar cells of pure sulfide (CZTS) composition has been recently reported also using co-electrodeposition (Ge and Yan, 2018).

The thermal treatment necessary to achieve high quality films can also be optimized by the use of rapid thermal processing (RTP). Prior work developed at IREC has demonstrated at lab scale the advantages of RTP systems in contrast to the most frequently used conventional thermal treatment (CTP) (Fairbrother et al., 2014). RTP is advantageous because processing times are much shorter than conventional thermal processes. By using RTP treatments, the total time of the selenized (sulfurized) stage can be reduced 5 times and even more, taking into account that an RTP takes minutes while a CTP takes hours of processing. Therefore, the incorporation of RTP treatments accomplish the premises that are sought for a large-scale process: speed, cost reduction and energy savings. RTP process has been mostly combined with kesterite precursors prepared by sputtering (He et al., 2014; Hwang et al., 2015; Olgar et al., 2017; Pawar et al., 2014; Placidi et al., 2016). On the side of electrochemical routes very little has been reported of the use of RTP processes. Vauche et al. have reported kesterites using electrodeposition of stacked layers (SEL method) followed by a RTP process (Vauche et al., 2014, 2015). It should be noted that the SEL method has significant experimental differences with the co-electrodeposition method (Colombara et al., 2015). On the side of the co-electrodeposition method.

In summary, this paper reports CZTSe thin films prepared by a sequential process combining a short-time co-electrodeposition of a CZT precursor and a selenization step with an RTP system. Selected films were tested in solar cell prototypes achieving a promising efficiency of 5.2% which is twice the efficiency of previous kesterite solar cells reported by the group using the co-electrodeposition route as a low cost approach (Kondrotas et al., 2015). To our best knowledge only one work has been published combining co-electrodeposition and RTP treatment, producing solar cells with 4.5% efficiency (Zhang et al., 2013). In contrast, the present work shows that even reducing 4 times the precursor electrodeposition time, solar cells with comparable (an even higher) efficiencies can be achieved.

2. Material and methods

CZTSe films were prepared by a sequential process onto Mo-coated soda lime glass substrates. First, a CuZnSn (CZT) precursor alloy was obtained by co-electrodeposition employing a three-electrode cell. Soda-lime glasses coated with a DC magnetron sputtered Mo layer were used as a working electrode. Prior to deposition, Mo substrates were

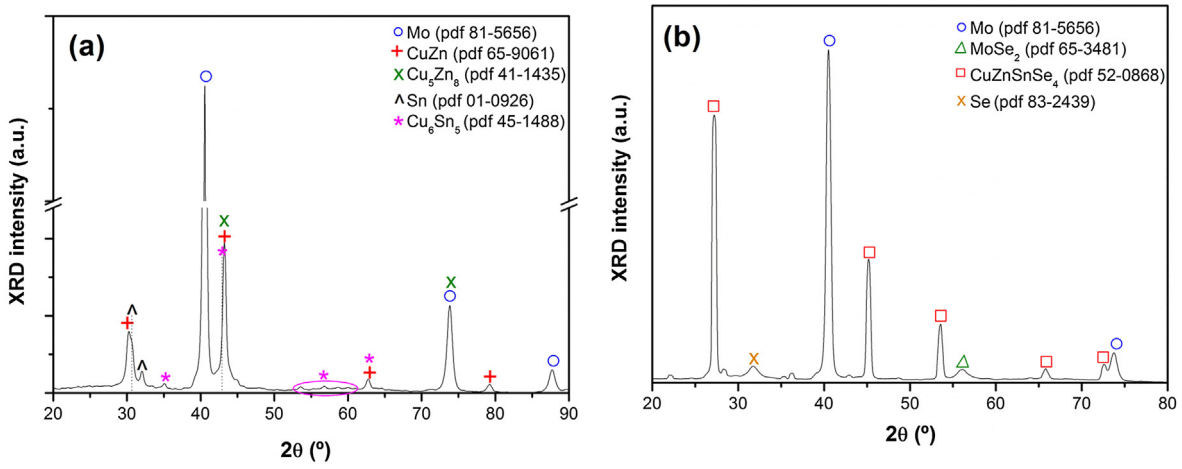

Fig. 2. XRD pattern of (a) CZT precursor electrodeposited at −1.2 V (vs. Ag/AgCl) during 15 min and (b) CZTSe thin film obtained after RTP treatment.

Table 1
Chemical composition and elements ratios in selected CZT and CZTSe films.[a]

Sample	Thickness [nm]	%Cu	%Zn	%Sn	%Se	Cu/(Zn + Sn)	Zn/Sn
CZT	480.5 ± 95.2	44.2 ± 1.1	27.9 ± 1.5	27.8 ± 1.1	–	0.79	1.00
Sample	Thickness [μm]	%Cu	%Zn	%Sn	%Se	Cu/(Zn + Sn)	Zn/Sn
CZTSe	1.65 ± 0.21	22.7 ± 1.2	14.1 ± 1.0	10.4 ± 0.3	52.8 ± 1.5	0.94	1.38
CZTSe + $KMnO_4$	1.62 ± 0.15	22.5 ± 0.9	12.9 ± 0.6	12.5 ± 0.5	52.1 ± 1.0	0.88	1.03
CZTSe + KMnO4 + $(NH_4)S$	1.55 ± 0.1	22.8 ± 0.6	13.2 ± 1.1	11.4 ± 0.4	52.6 ± 1.3	0.93	1.16
CZTSe + $KMnO_4$ + $(NH_4)S$ + KCN[b]	1.53 ± 0.15	21.4 ± 0.8	13. 6 ± 0.8	11.2 ± 0.6	53.8 ± 1.8	0.86	1.21

[a] Chemical composition and film thicknesses were determined using XRF. For CZT and CZTSe films the mean value and the error were calculated from six individual point measurements, while for the etched films not less than four individual measurements were taken.
[b] Composition of the best device reported in this work.

immersed in 20% NH_4OH solution for 3 min to remove native molybdenum oxide. A platinum (purity 99.999%) mesh of much larger dimensions than that of the working electrode was used as auxiliary electrode and a silver chloride electrode (Ag/AgCl, KCl saturated) served as reference.

The electrolyte solutions were prepared using deionized water containing milli molar concentrations of $CuSO_4{\cdot}5H_2O$ (ACS reagent ≥ 98% Sigma-Aldrich); $ZnSO_4{\cdot}7H_2O$ (ReagentPlus®, ≥99.0% Sigma-Aldrich) and $SnSO_4$ (≥95% Sigma-Aldrich). Sodium citrate tribasic ($Na_3C_6H_5O_7$, ACS reagent, ≥99.0% Sigma-Aldrich) was used as complexing agent in the electrolyte solution for the co-deposition of CZT as it was previously reported (Valdés et al., 2017). The molar ratios of Cu:Zn:Sn:Na-cit in the electrolyte were fixed to 1.3:1.2:1:20 with a copper concentration of 13×10^{-3} mol/L. The final pH of the solution was close to 6 without any addition of acids or bases. CZT precursor films were co-electrodeposited at room temperature in potentiostatic mode applying a potential of −1.2 V (vs. Ag/AgCl) during 15 min employing a VSP Electrochemical Workstation (Biologic).

In a second step, CZT precursors were selenized with a RTP system (AS-One AnnealSys). Samples were placed in a graphite box together with 25 mg of selenium powder (99.999 purity). The temperature profile employed is shown in Fig. 1. The total process time (heating + selenization steps + cooling) takes less than 30 min in a very controlled way, enabling important energy savings at industrial scale considering that RTP is the preferred thermal process in the thin film chalcogenide industry. The elemental composition and thicknesses of CZT and CZTSe films were measured by XRF (Fisherscope XVD) which has been previously calibrated by Inductively Coupled Plasma Optical Emission Spectroscopy (ICP).

The crystalline structure of the as-deposited metallic CZT precursors as well as of the selenized films was analyzed by X-ray diffraction using an Advance D8 diffraction system (Bruker) employing Cu Kα radiation at 40 kV and 40 mA. The samples were scanned, in Bragg-Brentano θ/2θ geometry, between 15° and 80° with a step size of 0.01°. Scanning electron microscopy (SEM) images were obtained using a ZEISS Series Auriga microscope. Raman scattering measurements were made using a Raman probe developed at IREC coupled with an optical fiber to an iHR320 Horiba Jobin Yvon spectrometer. The measurements were made in backscattering configuration focusing the excitation laser spot directly on the surface of the samples (diameter 50 μm, excitation power density < 1 kW/cm^2) with excitation wavelengths of 442 nm and 633 nm. Raman spectra were calibrated using a monocrystal Si reference sample before each measurement by imposing the position of the dominant Si peak at 520 cm^{-1}. Raman micro-mappings were performed using an Invia Reflex confocal Raman microprobe using a 50× objective. Excitation was provided with the 514 nm emission line of an Ar^+ laser and 786 nm emission of IR-laser. The laser power on the sample was less than 2 mW measured with a silicon photodiode (Coherent Inc.). Maps were obtained scanning a square zone (100 × 100 μm) in the sample and recording a total of 25 spectra in the x and y directions. For both axes the step between spectra was set in 20 μm.

After a through characterization, the films were incorporated into solar cells. Selected films were etched in a series of electrolytes: in an acidic solution of $KMnO_4$, to remove superficially segregated ZnSe (López-Marino et al., 2013b), in NaS_2 solution to remove SnSe and passivate the surface region (Xie et al., 2014); and finally in 2 wt.%/v KCN solution to remove possible Cu_xSe secondary phases. An n-type buffer layer of CdS was deposited by chemical bath deposition to a thickness of approximately 50 nm as is published in (Neuschitzer et al., 2015). Immediately after the CdS growth, the solar cells were completed by DC-pulsed sputtering deposition (Alliance CT100) of i-ZnO (50 nm) and In:SnO_2 (ITO, 350 nm) as transparent window layer and front conductive layer, respectively. The CZTSe/CdS junction was not intentionally heated until the deposition of the ITO layer which is performed at 200 °C in the sputtering system. Afterwards, for the standard optoelectronic characterization, 3 × 3 mm^2 cells were mechanically scribed using a manual microdiamond scriber (MR200, OEG Optical Metrology). Dark and illuminated J–V curves were measured using a calibrated Sun 3000 class AAA solar simulator (Abet Technologies). Measurements were carried out at 25 °C, under AM1.5G 1-Sun illumination conditions. The spectral response was measured using a Bentham PVE300 system calibrated with Si and Ge photodiodes, in order to obtain the EQE of the solar cells.

3. Results and discussion

Fig. 2 presents the XRD diffractograms of a CZT precursor (Fig. 2a) and a CZTSe film after RTP selenization (Fig. 2b). The precursor is mainly composed of CuZn, zinc-rich Cu_5Zn_8 and Cu_6Sn_5 intermetallic compounds. Also, weak signals assigned to elemental Sn are also observed. These phases are frequently observed in co-electrodeposited CZT films, given that as confirmed by several authors (Gougaud et al., 2013; Hreid et al., 2015; Juškenas et al., 2012; Schurr et al., 2009), the co-electrodeposition route involves the formation of alloys instead of pure metals. The presence of intermetallic CuZn has been related to a Cu-poor composition of the CZT precursor (Schurr et al., 2009) and as it was reported by Hreid et al., the concentration of Cu ions regulates the formation of intermetallic compounds (Hreid et al., 2015).

After RTP (Fig. 2b), the film presents intense and sharp peaks of the

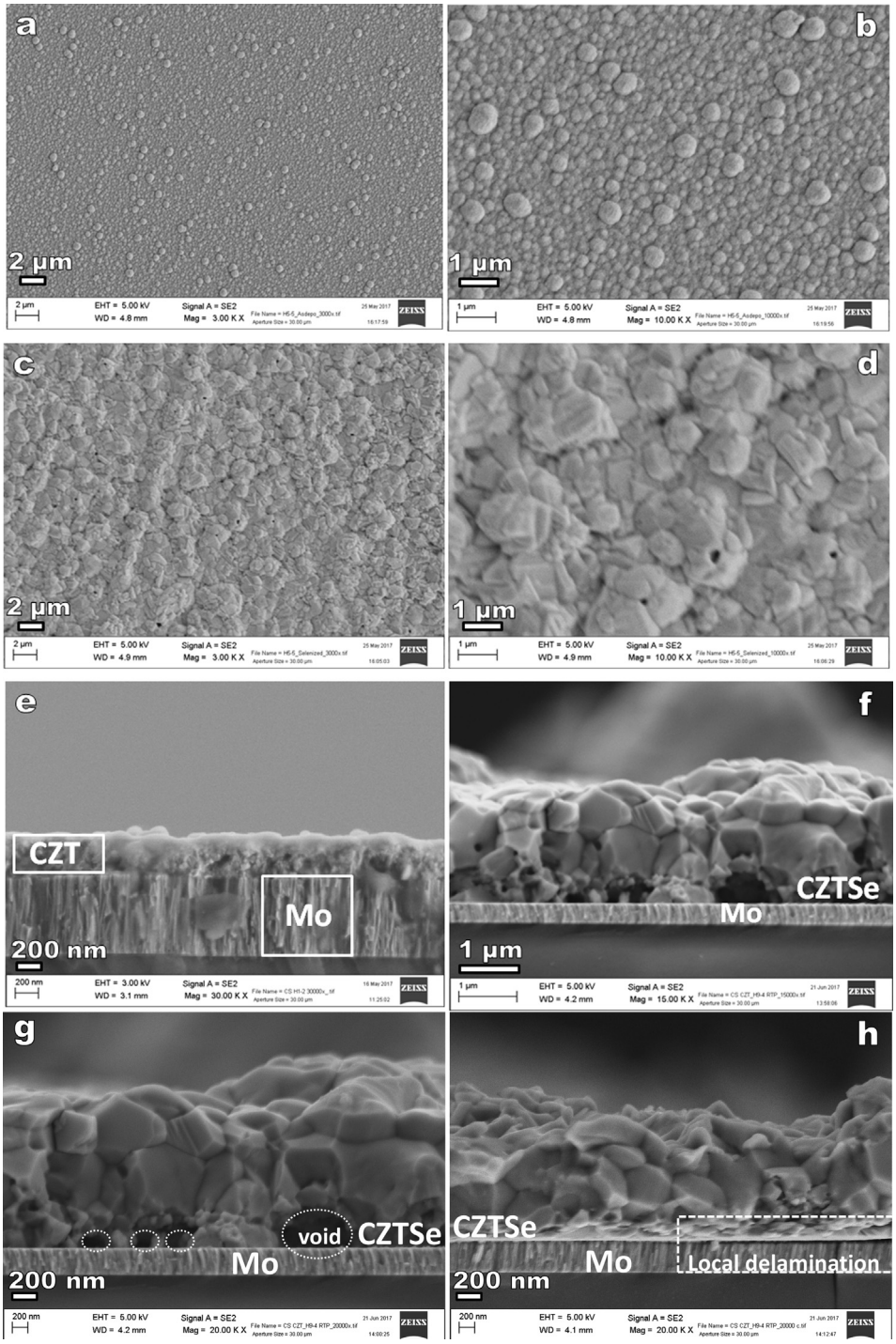

Fig. 3. Top-view FESEM pictures of (a-b) co-electrodeposited CZT precursor (c-d) CZTSe thin film obtained after RTP selenization. Cross section view of (e) CZT precursor and (f-h) CZTSe thin films (no etching). Pictures (g-h) show defects at Mo/CZTSe interface using higher magnification.

main crystallographic planes of the CZTSe phase. Minor signals of $MoSe_2$ and elemental Se are also observed. The former is attributed to the formation of a $MoSe_2$ layer during selenization. According to Wei et al, during the cooling down of the annealing process residual selenium on the samples can be deposit by condensation of Se vapor (Wei et al., 2018).

Further than the crystal structure, another important factor for achieving working devices is the chemical composition, particularly the Cu/(Zn + Sn) and Zn/Sn ratios. It has been well established that highly efficient devices must present a Cu-poor and Zn-rich composition, and so must the precursor. Table 1 presents the chemical composition of the CZT precursor, of the CZTSe films after RTP and the composition after chemical etching. The composition of the precursor fulfills the pre-requisites of Cu-poor, and presents equal contents of zinc and tin atoms.

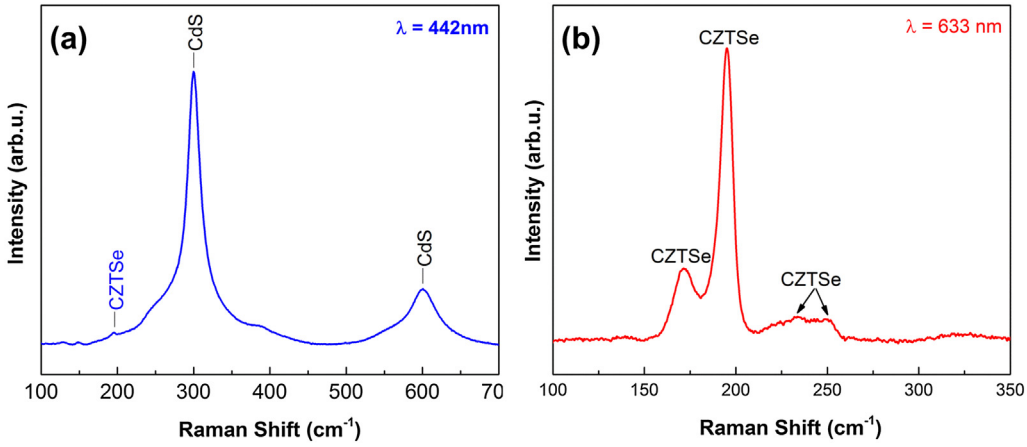

Fig. 4. Raman spectra of a finished solar cell under different excitation wavelengths: (a) 442 nm and (b) 633 nm.

The thickness of the CuZnSn precursor is close to 0.5 μm but the dispersion of this value, which is related to the thickness homogeneity, is relatively high. This is likely to be one of the main drawbacks of the co-electrodeposition approach (Colombara et al., 2015). Despite this, the deviation in the chemical composition of each element is less than 5%, which for a 2.5 × 2.5 cm^2 electrodeposited film indicates good uniformity. After RTP and selenium incorporation the composition is slightly Cu-poor and Zn-rich. The excess of selenium (above 50%) is attributed to the $MoSe_2$ layer during selenization and elemental selenium, in accordance with what was observed by XRD.

Table 1 also includes the change in the atomic composition of the CZTSe film after being etched in selected solutions to remove secondary phases like ZnSe, Sn-Se and Cu_xSe. After the etchings, the composition of the best CZTSe absorber gives a Cu/(Zn + Sn) ~ 0.85 and (Zn/Sn) ~ 1.2. The thickness of the CZTS film is in average three times higher than the precursor material. This expansion of the films is usually observed in reactive annealing, mainly, where the chalcogen is incorporated into the material during the thermal treatment (Ahmed et al., 2012; Jeon et al., 2014; Salomé et al., 2010; Scragg, 2011). Selected FESEM images are presented in Fig. 3. At low magnification (Fig. 3a) the films appear to be homogenously deposited and no voids or cracks are observed. Indeed, after co-electrodeposition, CZT precursors present specular reflectivity.

At higher magnification (Fig. 3b), round particles (or agglomerates) can be visualized in the nanometer range, with some dispersion of bigger agglomerates at the top surface. After the RTP treatment (Fig. 3c) the material continues to present a high degree of homogeneity but the morphology fully changes to planar particles with irregular shape. Now, CZTSe absorbers do not longer show a shiny specular surface and transform into to a grayish and opaque film. At higher magnification (Fig. 3d) small voids are observed on the surface of the CZTSe film. These could be produced by partial evaporation of volatile compounds formed at high temperatures like $SnSe_x$ (López-Marino et al., 2013a; Márquez et al., 2017; Redinger et al., 2011; Salomé et al., 2010). As it can be seen in Table 1, the increase of the Zn/Sn ratio from 1 to 1.38 after RTP is an indication of tin evaporation during RTP. In a recent work, Unveroglu et al. have reported a similar behavior of tin evaporation during sulfurization of co-electrodeposited CZT precursors quantifying the variation of the Zn/Sn ratio before and after the thermal treatment (Unveroglu and Zangari, 2016). Cross section pictures of CZT (Fig. 3e) and CZTSe films (Fig. 3f) corroborate the XRF thickness measurements and, in fact, provide additional evidence of the volume expansion in the film after the RTP treatment. The CZT precursor shows compactness and high adherence to the Mo substrate while after RTP some voids in the Mo/CZTSe interface are present. Localized delamination (partial detachment of kesterite from the substrate) is highly detrimental for device performance because a low quality Mo/CZTSe interface strongly influences overall solar cell performance, especially decreases shunt resistance affecting the open circuit voltage.

The formation of voids or local delamination has been reported before in kesterite films synthesized from electrodeposited precursors (Guo et al., 2014; Kondrotas et al., 2015; Li et al., 2014; Vauche et al., 2014), but it is a common problem that extends to other fabrication techniques like sputtering (Malerba et al., 2016; Márquez et al., 2017) or chemical methods (Larramona et al., 2014; Todorov et al., 2013).

Raman spectra of a complete solar cell are presented in Fig. 4. Different laser wavelengths were used to identify potential secondary phases taking into account Raman resonant excitation. For CZTSe, resonant effects are frequently found in binary compounds like ZnSe and Sn-Se, at excitation laser wavelengths of 442 and 633 nm, respectively (Álvarez-García et al., 2016). After the chemical etchings of the CZTSe absorber, no traces of $SnSe_2$ and ZnSe secondary phases were observed. Fig. 4a presents a Raman spectrum of a complete device using 442 nm excitation wavelength. The spectrum is characterized by the dominant band at 300 cm^{-1} identified as A_1(LO) of the CdS, and weaker contributions at around 195 and 600 cm^{-1} identified as Se–Se vibrations of the CZTSe and the second order of the A_1 (LO) CdS mode. Resonant effects of CdS at this laser wavelength explain the remarkable difference in Raman intensities between CdS ad CZTSe layers (Oliva et al., 2016). On the other hand, the absence of contributions at 250 and 500 cm^{-1} characteristics of ZnSe under resonant conditions (488 nm) suggest the absence of this phase in the CZTSe surface (Dimitrievska et al., 2016). With a laser excitation of 633 nm (Fig. 4b) only Raman signals coming from the CZTSe layer are present in the spectrum without interference of the upper layers (Oliva et al., 2016). The spectrum presents two main modes of CZTSe at 195 cm^{-1} and at 170 cm^{-1}, both with A symmetry; and other two minor signals at 235 and 250 cm^{-1} with E and B symmetry, as it is reported in the literature (Guc et al., 2013). Under these excitation conditions the absence of the Raman signals between 110 and 180 cm^{-1} can be taken as an indication of the absence of Sn-Se related secondary phases on the surface film (Dimitrievska et al., 2016).

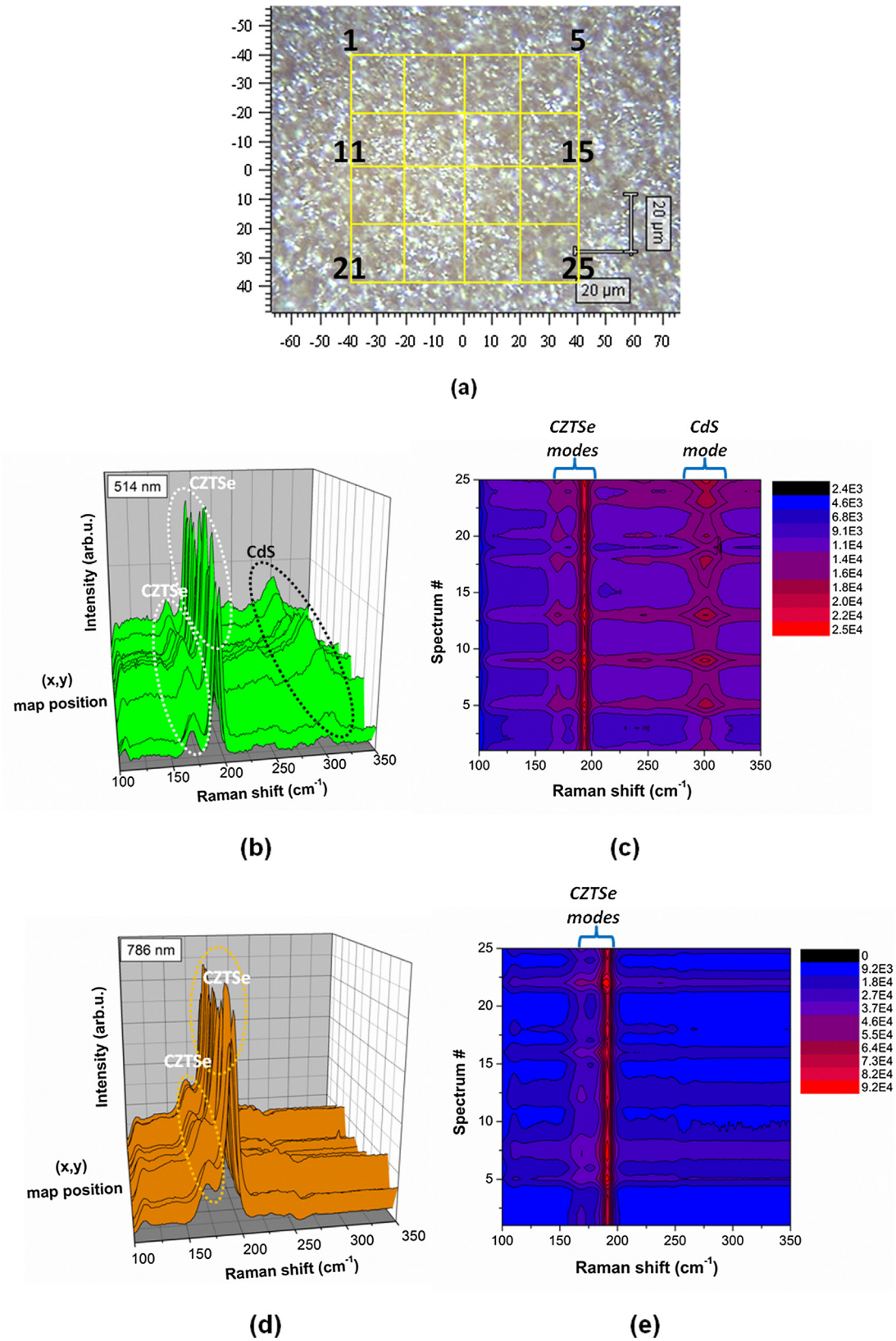

Fig. 5. Raman μ-maps of the best CZTSe sample reported in this work; (a) microscopy image and grid used to record the maps; (b) 514 nm Raman map; (c) 514 nm color contour of Raman intensity signals; (d) 786 nm Raman map and (e) 786 nm color contour of Raman intensity signals. (For interpretation of the references to colour in this figure legend, the reader is referred to the web version of this article.)

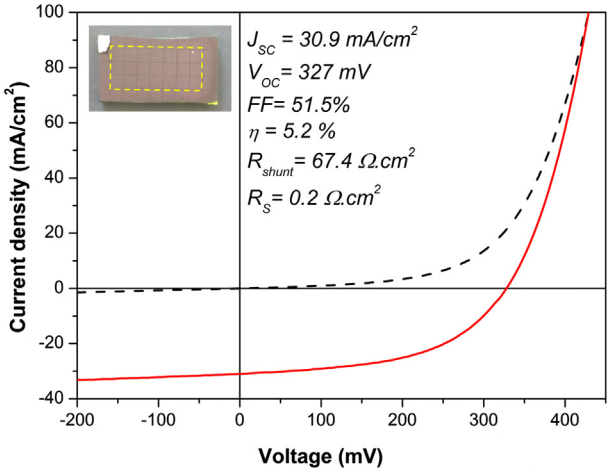

Fig. 6. Current-voltage curves recorded under simulated AM1.5G for the best CZTSe solar cells prototype. The insert shows an image of a full sample and the cells that were measured for the statistical values presented in Table 2.

Raman micro-mapping has emerged as powerful tool to study the homogeneity of thin films and their properties. Raman maps were recorded following the grid presented in Fig. 5a, using 20 μm steps in the x and y directions. Raman maps performed at excitation wavelengths of 532 (Fig. 5b and c) and 786 nm (Fig. 5d and d) show a homogenous distribution of kesterite Raman signals along the analyzed area (80 × 80 μm) together with a small and broad signal of the CdS buffer layer, that is only visible when the excitation is made with the 514 nm (close to the resonant effect). The broadening of the CdS Raman mode is explained by its nanocrystalline dimensions. The even distribution of Raman signals and a more statistical representation can be visualized when the maps are shown in the form of colors contour. These are presented in Fig. 5c and d for each wavelength, respectively. In both figures can be observed narrows and high intensity color bands around the main A mode (195 cm^{-1}) of the CZTSe, which is an indication of high crystallinity and homogeneity of the CZTSe absorber throughout the whole sample.

I-V curves of the best device in the dark and in simulated AM1.5 solar radiation are shown in Fig. 6. Extracted solar cell parameters for the best cell, and statistical values for the full sample (see insert in Fig. 5), are presented in Table 2. A solar cell with a maximum efficiency (η) of 5.2% was achieved, which is twice the efficiency of previous devices reported by our group using co-electrodeposition (Kondrotas et al., 2015). Shunt and series resistance for the best cell were R_{shunt} = 67.4 Ω cm^2 and R_s = 0.2 Ω cm^2 respectively. As it was expected from the observation of the Mo/CZTSe interface, the R_{shunt} of the solar cell is very low compared to higher efficiency cells (typically 10 times higher) (Giraldo et al., 2015; Wang et al., 2014). The low R_{shunt} value is originated by the presence of defects in the Mo/CZTSe interface reducing the fill factor and V_{OC} of the cell. A soft pre-annealing of the CZT/Mo (Lin et al., 2014) or back contact modification (López-Marino et al., 2013a) could help to reduce these defects in the interface.

It is important to notice that there is no crossover between dark and illuminated I-V curves. The explanation of crossover of I-V curves in CZTSe solar cells has been ascribed mainly to photogenerated carrier trapping in the CdS layer (Ben Messaoud et al., 2015; Khadka et al., 2016; Neuschitzer et al., 2015). Therefore, the absence of a crossover can be taken as a proof of a proper CZTSe/CdS interface quality and band alignment.

An external quantum efficiency (EQE) spectrum of the best cell is depicted in Fig. 7. EQE reaches 70–80% between 500 and 800 nm indicating reasonably good carrier generation and collection in the p-n junction. Below 500 nm absorption of the CdS buffer layer reduces the EQE in this region. From 900 nm, the decay in EQE could be related to a low diffusion length of carrier generated at these wavelengths.

In comparison with the work previously published by the group (Kondrotas et al., 2015), in this work replacing (time consuming) conventional thermal treatment with RTP we have improved the quality of CZTSe films. This has led us to double the efficiency of the cells, improving the electrical parameters of the devices. The series resistance (R_s) of the cells has decreased an order of magnitude, increasing the Jsc and the FF. On the other hand, the shunt resistance (R_{shunt}) of our cells is still low compared to record devices limiting the V_{OC} of our cells. An improvement of the Mo/CZTSe interface is essential to achieve this objective and obtain greater efficiencies.

4. Conclusion

CZTSe thin films were synthesized combining the co-electrodeposition of a CuZnSn (CZT) precursor with a rapid thermal (selenization) process. CZT films mainly consisted in binary CuZn and CuSn phases. FESEM pictures revealed that the films were homogeneous and formed by round particles (or agglomerates) in the nanometer range. After the RTP treatment, the morphology fully changes to platelet-shaped grains. Cross-section FESEM pictures exposed different types of defects located in the Mo/CZTSe interface like voids and partial film delamination which act as recombination paths affecting device performance. Selected films were submitted to several etchings in order to remove detrimental secondary phases and adjust the chemical composition. The best device reported in this work achieved a 5.2% conversion efficiency, which doubles the solar cells efficiency previously reported by the group using co-electrodeposition. The main limitation of this device is the low open circuit (V_{OC}) potential of 327 mV in comparison with record CZTSe devices. The low V_{OC} value is highly related to the low quality of the Mo/CZTSe interface. A soft-annealing treatment prior the RTP (improving precursor quality) or introducing back contact modification can help to mitigate interface defects and improve device efficiency. Work in this direction is currently in progress.

Table 2
CZTS best device optoelectronic parameters.[a]

η (best) [%]	η (mean) [%]	RSD [%]	J_{sc} (best) [mA cm^{-2}]	J_{sc} (mean) [mA cm^{-2}]	RSD [%]	V_{oc} (best) [mV]	V_{oc} (mean) [mV]	RSD [%]	FF [%]	R_{SH} [Ω cm^2]	R_S [Ω cm^2]
5.2	4.5	11.7	30.9	30.8	4.7	327	309.9	5.4	46.7	48.5	0.8

RSD, relative standard deviation.

[a] Main optoelectronic parameters (η, V_{OC}, J_{SC}) are reported as best value at cell size (active area: 0.087 cm^2), average value for the full sample (21 cells, see insert in Fig. 5a), and its relative standard deviation. The reported values for fill factor (FF), series (R_S), and shunt resistance (R_{SH}) are average for the full sample.

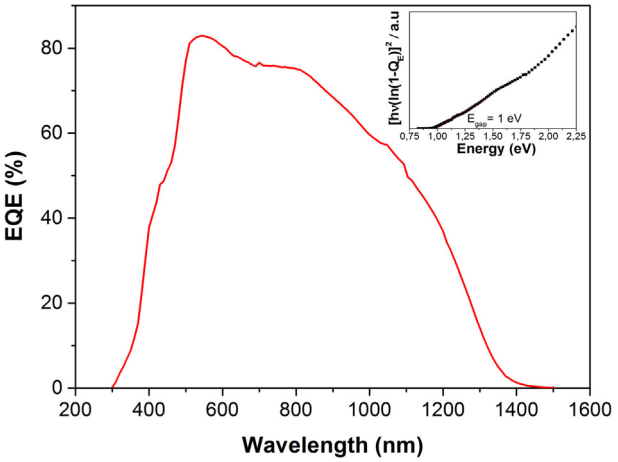

Fig. 7. External quantum efficiency (EQE) of the best device. The inset shows the calculated energy gap (E_{GAP}) of the CZTSe absorber from the EQE data.

Acknowledgements

M. Valdes knowledges the financial support of Consejo Nacional de Investigaciones Científicas y Técnicas (CONICET, Argentina) under the External Fellowship Program for young researchers and the Universidad Nacional de Mar del Plata (UNMdP, Argentina). This research was supported by MINECO (Ministerio de Economía y Competitividad de España) under the NASCENT project (ENE2014-56237-C4-1-R). A.H.M. thanks the Government of Spain for the FPI fellowship (BES-2015-074171).

References

Ahmed, S., Reuter, K.B., Gunawan, O., Guo, L., Romankiw, L.T., Deligianni, H., 2012. A high efficiency electrodeposited cu2znsns4 solar cell. Adv. Energy Mater. 2 (2), 253–259.

Almosni, S., Delamarre, A., Jehl, Z., Suchet, D., Cojocaru, L., Giteau, M., Behaghel, B., Julian, A., Ibrahim, C., Tatry, L., Wang, H., Kubo, T., Uchida, S., Segawa, H., Miyashita, N., Tamaki, R., Shoji, Y., Yoshida, K., Ahsan, N., Watanabe, K., Inoue, T., Sugiyama, M., Nakano, Y., Hamamura, T., Toupance, T., Olivier, C., Chambon, S., Vignau, L., Geffroy, C., Cloutet, E., Hadziioannou, G., Cavassilas, N., Rale, P., Cattoni, A., Collin, S., Gibelli, F., Paire, M., Lombez, L., Aureau, D., Bouttemy, M., Etcheberry, A., Okada, Y., Guillemoles, J.-F., 2018. Material challenges for solar cells in the twenty-first century: directions in emerging technologies. Sci. Technol. Adv. Mater. 19 (1), 336–369.

Álvarez-García, J., Izquierdo-Roca, V., Pistor, P., Schmid, T., Pérez-Rodríguez, A., 2016. In: Raman Spectroscopy on Thin Films for Solar Cells, Advanced Characterization Techniques for Thin Film Solar Cells. Wiley-VCH Verlag GmbH & Co. KGaA, pp. 469–499.

Ben Messaoud, K., Buffière, M., Brammertz, G., ElAnzeery, H., Oueslati, S., Hamon, J., Kniknie, B.J., Meuris, M., Amlouk, M., Poortmans, J., 2015. Impact of the Cd^{2+} treatment on the electrical properties of $Cu_2ZnSnSe_4$ and Cu(In, Ga)S_e2 solar cells. Prog. Photovolt: Res. Appl. 23 (11), 1608–1620.

Colombara, D., Crossay, A., Vauche, L., Jaime, S., Arasimowicz, M., Grand, P.P., Dale, P.J., 2015. Electrodeposition of kesterite thin films for photovoltaic applications: Quo vadis? Phys. Stat. Solidi A 88–102.

Dimitrievska, M., Fairbrother, A., Saucedo, E., Pérez-Rodríguez, A., Izquierdo-Roca, V., 2016. Secondary phase and Cu substitutional defect dynamics in kesterite solar cells: impact on optoelectronic properties. Sol. Energy Mater. Sol. Cells 149, 304–309.

Djokić, S.S., 2014. In: Electrodeposition and Surface Finishing, Modern Aspects of Electrochemistry. Springer-Verlag, New York, pp. pp. XIV 363.

Fairbrother, A., Fourdrinier, L., Fontané, X., Izquierdo-Roca, V., Dimitrievska, M., Pérez-Rodríguez, A., Saucedo, E., 2014. Precursor stack ordering effects in $Cu_2ZnSnSe_4$ thin films prepared by rapid thermal processing. J. Phys. Chem. C 118 (31), 17291–17298.

Ge, J., Yan, Y., 2018. Controllable multinary alloy electrodeposition for thin-film solar cell fabrication: a case study of kesterite Cu_2ZnSnS_4. iScience 1, 55–71.

Giraldo, S., Neuschitzer, M., Thersleff, T., Lõpez-Marino, S., Sánchez, Y., Xie, H., Colina, M., Placidi, M., Pistor, P., Izquierdo-Roca, V., Leifer, K., Pérez-Rodríguez, A., Saucedo, E., 2015. Large efficiency improvement in $Cu_2ZnSnSe_4$ solar cells by introducing a superficial Ge nanolayer. Adv. Energy Mater. 5 (21).

Giraldo, S., Saucedo, E., Neuschitzer, M., Oliva, F., Placidi, M., Alcobé, X., Izquierdo-Roca, V., Kim, S., Tampo, H., Shibata, H., Pérez-Rodríguez, A., Pistor, P., 2018. How small amounts of Ge modify the formation pathways and crystallization of kesterites. Energy Environ. Sci. 11 (3), 582–593.

Gougaud, C., Rai, D., Delbos, S., Chassaing, E., Lincot, D., 2013. Electrochemical studies of one-step electrodeposition of Cu-Sn-Zn layers from aqueous electrolytes for photovoltaic applications. J. Electrochem. Soc. 160 (10), D485–D494.

Guc, M., Levcenko, S., Izquierdo-Roca, V., Fontané, X., Arushanov, E., Pérez- Rodríguez, A., 2013. Polarized Raman scattering analysis of $Cu_2ZnSnSe_4$ and $Cu_2ZnGeSe_4$ single crystals. J. Appl. Phys. 114 (19).

Guo, L., Zhu, Y., Gunawan, O., Gokmen, T., Deline, V.R., Ahmed, S., Romankiw, L.T., Deligianni, H., 2014. Electrodeposited $Cu_2ZnSnSe_4$ thin film solar cell with 7% power conversion efficiency. Prog. Photovolt.: Res. Appl. 22 (1), 58–68.

He, J., Sun, L., Chen, Y., Jiang, J., Yang, P., Chu, J., 2014. Cu_2ZnSnS_4 thin film solar cell utilizing rapid thermal process of precursors sputtered from a quaternary target: a promising application in industrial processes. RSC Adv. 4 (81), 43080–43086.

Hreid, T., Li, J., Zhang, Y., Spratt, H.J., Wang, H., Will, G., 2015. Effects of metal ion concentration on electrodeposited CuZnSn film and its application in kesterite Cu_2ZnSnS_4 solar cells. RSC Adv. 5 (80), 65114–65122.

Hwang, S., Kim, D.H., Son, D.H., Yang, K.J., Nam, D., Cheong, H., Kang, J.K., In, S.I., 2015. Effects of a pre-annealing treatment (PAT) on $Cu_2ZnSn(S, Se)_4$ thin films prepared by rapid thermal processing (RTP) selenization. Sol. Energy Mater. Sol Cells 143, 218–225.

Jeon, J.-O., Lee, K.D., Seul Oh, L., Seo, S.-W., Lee, D.-K., Kim, H., Jeong, J.-h., Ko, M.J., Kim, B., Son, H.J., Kim, J.Y., 2014. Highly efficient copper–zinc–tin– selenide (CZTSe) solar cells by electrodeposition. ChemSusChem 7(4), 1073–1077.

Jiang, F., Ikeda, S., Harada, T., Matsumura, M., 2014. Pure Sulfide Cu_2ZnSnS_4 thin film solar cells fabricated by preheating an electrodeposited metallic stack. Adv. Energy Mater. 4 (7), 1301381.

Juškenas, R., Kanapeckaite, S., Karpavičiene, V., Mockus, Z., Pakštas, V., Selskiene, A., Giraitis, R., Niaura, G., 2012. A two-step approach for electrochemical d eposition of Cu-Zn-Sn and Se precursors for CZTSe solar cells. Sol. Energy Mater. Sol. Cells 101, 277–282.

Khadka, D.B., Kim, S., Kim, J., 2016. Effects of Ge alloying on device characteristics of kesterite-based CZTSSe thin film solar cells. J. Phys. Chem. C 120 (8), 4251–4258.

Khalil, M.I., Bernasconi, R., Pedrazzetti, L., Lucotti, A., Donne, A.L., Binetti, S., Magagnin, L., 2017. Co-electrodeposition of metallic precursors for the fabrication of CZTSe thin films solar cells on flexible Mo foil. J. Electrochem. Soc. 164 (6), D302–D306.

Kim, G.Y., Jo, W., Lee, K.D., Choi, H.S., Kim, J.Y., Shin, H.Y., Nguyen, T.T.T., Yoon, S., Joo, B.S., Gu, M., Han, M., 2015. Optical and surface probe investigation of secondary phases in Cu_2ZnSnS_4 films grown by electrochemical deposition. Sol. Energy Mater. Sol Cells 139, 10–18.

Kondrotas, R., Juškėnas, R., Naujokaitis, A., Selskis, A., Giraitis, R., Mockus, Z., Kanapeckaitė, S., Niaura, G., Xie, H., Sánchez, Y., Saucedo, E., 2015. Characterization of $Cu_2ZnSnSe_4$ solar cells prepared from electrochemically co-deposited Cu–Zn–Sn alloy. Sol. Energy Mater. Sol. Cells 132, 21–28.

Larramona, G., Bourdais, S., Jacob, A., Choné, C., Muto, T., Cuccaro, Y., Delatouche, B., Moisan, C., Péré, D., Dennler, G., 2014. Efficient Cu_2ZnSnS_4 solar cells spray coated from a hydro-alcoholic colloid synthesized by instantaneous reaction. RSC Adv. 4 (28), 14655–14662.

Li, Y., Yuan, T., Jiang, L., Su, Z., Liu, F., 2014. Growth and characterization of Cu_2ZnSnS_4 photovoltaic thin films by electrodeposition and sulfurization. J. Alloys Compd. 610, 331–336.

Lin, Y., Ikeda, S., Septina, W., Kawasaki, Y., Harada, T., Matsumura, M., 2014. Mechanistic aspects of preheating effects of electrodeposited metallic precursors on structural and photovoltaic properties of Cu_2Zn SnS_4 thin films. Sol. Energy Mater. Sol. Cells 120 (PART A), 218–225.

López-Marino, S., Placidi, M., Pérez-Tomás, A., Llobet, J., Izquierdo-Roca, V., Fontané, X., Fairbrother, A., Espíndola-Rodríguez, M., Sylla, D., Pérez- Rodríguez, A., Saucedo, E., 2013a. Inhibiting the absorber/Mo-back contact decomposition reaction in $Cu_2ZnSnSe_4$ solar cells: the role of a ZnO intermediate nanolayer. J. Mater. Chem. A 1 (29), 8338–8343.

López-Marino, S., Sánchez, Y., Placidi, M., Fairbrother, A., Espindola-Rodríguez, M., Fontané, X., Izquierdo-Roca, V., López-García, J., Calvo-Barrio, L., Pérez- Rodríguez, A., Saucedo, E., 2013b. ZnSe etching of Zn-Rich $Cu_2ZnSnSe_4$: an oxidation route for improved solar-cell efficiency. Chem. Eur. J. 19 (44), 14814–14822.

Malerba, C., Valentini, M., Azanza Ricardo, C.L., Rinaldi, A., Cappelletto, E., Scardi, P., Mittiga, A., 2016. Blistering in Cu_2ZnSnS_4 thin films: correlation with residual stresses. Mater. Des. 108, 725–735.

Márquez, J., Stange, H., Hages, C.J., Schaefer, N., Levcenko, S., Giraldo, S., Saucedo, E., Schwarzburg, K., Abou-Ras, D., Redinger, A., Klaus, M., Genzel, C., Unold, T., Mainz, R., 2017. Chemistry and dynamics of Ge in kesterite: toward band-gap-graded absorbers. Chem. Mater. 29 (21), 9399–9406.

Neuschitzer, M., Sanchez, Y., Lõpez-Marino, S., Xie, H., Fairbrother, A., Placidi, M., Haass, S., Izquierdo-Roca, V., Perez-Rodriguez, A., Saucedo, E., 2015. Optimization of CdS buffer layer for high-performance $Cu_2ZnSnSe_4$ solar cells and the effects of light soaking: elimination of crossover and red kink. Prog. Photovolt.: Res. Appl. 23 (11), 1660–1667.

Olgar, M.A., Klaer, J., Mainz, R., Ozyuzer, L., Unold, T., 2017. Cu_2ZnSnS_4-based thin films and solar cells by rapid thermal annealing processing. Thin Solid Films 628, 1–6.

Oliva, F., Kretzschmar, S., Colombara, D., Tombolato, S., Ruiz, C.M., Redinger, A., Saucedo, E., Broussillou, C., de Monsabert, T.G., Unold, T., Dale, P.J., Izquierdo-Roca, V., Pérez-Rodríguez, A., 2016. Optical methodology for process monitoring of chalcopyrite photovoltaic technologies: application to low cost Cu(In,Ga)(S,Se)2 electrodeposition based processes. Sol. Energy Mater. Sol. Cells 158 (Part 2), 168-183.

Pawar, S.M., Inamdar, A.I., Pawar, B.S., Gurav, K.V., Shin, S.W., Yanjun, X., Kolekar, S.S., Lee, J.H., Kim, J.H., Im, H., 2014. Synthesis of Cu_2ZnSnS_4 (CZTS) absorber by rapid thermal processing (RTP) sulfurization of stacked metallic precursor films for solar cell applications. Mater. Lett. 118, 76–79.

Placidi, M., Espindola-Rodriguez, M., Lopez-Marino, S., Sanchez, Y., Giraldo, S., Acebo, L., Neuschitzer, M., Alcobé, X., Pérez-Rodríguez, A., Saucedo, E., 2016. Effect of rapid

thermal annealing on the Mo back contact properties for $Cu_2ZnSnSe_4$ solar cells. J. Alloys Compd. 675, 158–162.
Platzer-Björkman, C., 2017. Kesterite compound semiconductors for thin film solar cells. Curr. Opin. Green Sustain. Chem. 4, 84–90.
Popov, K.I., Djokić, S.S., Nikolicć, N.D., Jović, V.D., 2016. Morphology of Electrochemically and Chemically Deposited Metals. Springer International Publishing.
Rakhshani, A.E., Bumajdad, A., Al-Sagheer, F., Thomas, S., Tharayil, P.H., 2017. One-step electrodeposition of CuZnSn metal alloy precursor film followed by the synthesis of $Cu_2ZnSnS_4$and $Cu_2ZnSnSe_4$ light absorber films and heterojunction devices. Int. J. Electrochem. Sci. 12 (8), 7786–7794.
Redinger, A., Berg, D.M., Dale, P.J., Siebentritt, S., 2011. The consequences of kesterite equilibria for efficient solar cells. J Am. Chem. Soc. 133 (10), 3320–3323.
Salomé, P.M.P., Fernandes, P.A., Da Cunha, A.F., 2010. Influence of selenization pressure on the growth of $Cu_2ZnSnSe_4$ films from stacked metallic layers. Phys. Stat. Solidi (C) 7 (3–4), 913–916.
Scragg, J.J., 2011. Copper Zinc Tin Sulfide Thin Films for Photovoltaics. Springer, Berlin.
Schurr, R., Hölzing, A., Jost, S., Hock, R., Voß, T., Schulze, J., Kirbs, A., Ennaoui, A., Lux-Steiner, M., Weber, A., Kötschau, I., Schock, H.W., 2009. The crystallisation of Cu_2ZnSnS_4 thin film solar cell absorbers from co-electroplated Cu-Zn-Sn precursors. Thin Solid Films 517 (7), 2465–2468.
Siebentritt, S., 2017. High voltage, please!. Nat. Energy 2 (11), 840–841.
Todorov, T.K., Tang, J., Bag, S., Gunawan, O., Gokmen, T., Zhu, Y., Mitzi, D.B., 2013. Beyond 11% efficiency: characteristics of state-of-the-art $Cu_2ZnSn(S, Se)_4$ Solar Cells. Adv. Energy Mater. 3 (1), 34–38.
Unveroglu, B., Zangari, G., 2016. Towards phase pure kesterite CZTS films via Cu-Zn- Sn electrodeposition followed by sulfurization. Electrochim. Acta 219, 664–672.
Valdés, M., Di Iorio, Y., Castañeda, K., Marotti, R.E., Vázquez, M., 2017. Cu_2ZnSnS_4 thin films prepared by sulfurization of co-electrodeposited metallic precursors. J. Appl. Electrochem. 47 (6), 755–765.
Vauche, L., Dubois, J., Laparre, A., Mollica, F., Bodeux, R., Delbos, S., Ruiz, C.M., Pasquinelli, M., Bahi, F., de Monsabert, T.G., Jaime, S., Bodnar, S., Grand, P.P., 2014. $Cu_2ZnSnSe_4$ thin film solar cells above 5% conversion efficiency from electro-deposited Cu Sn Zn precursors. Phys. Stat. Solidi (a) 211 (9), 2082–2085.
Vauche, L., Dubois, J., Laparre, A., Pasquinelli, M., Bodnar, S., Grand, P.-P., Jaime, S., 2015. Rapid thermal processing annealing challenges for large scale Cu_2ZnSnS_4 thin films. Phys. Stat. Solidi (a) 212 (1), 103–108.
Vauche, L., Risch, L., Sánchez, Y., Dimitrievska, M., Pasquinelli, M., Goislard De Monsabert, T., Grand, P.P., Jaime-Ferrer, S., Saucedo, E., 2016. 8.2% pure selenide kesterite thin-film solar cells from large-area electrodeposited precursors. Prog. Photovolt.: Res. Appl. 24 (1), 38–51.
Wallace, S.K., Mitzi, D.B., Walsh, A., 2017. The steady rise of kesterite solar cells. ACS Energy Lett. 2 (4), 776–779.
Wang, W., Winkler, M.T., Gunawan, O., Gokmen, T., Todorov, T.K., Zhu, Y., Mitzi, D.B., 2014. Device characteristics of CZTSSe thin-film solar cells with 12.6% efficiency. Adv. Energy Mater. 4 (7), 1301465.
Wei, Y., Zhuang, D., Zhao, M., Gong, Q., Sun, R., Zhang, L., Lyu, X., Peng, X., Ren, G., Wu, Y., Wei, J., 2018. Effects of selenium atmosphere on grain growth for CZTSe absorbers fabricated by selenization of as-sputtered precursors. J. Alloys Compd. 755, 224–230.
Xie, H., Sánchez, Y., López-Marino, S., Espíndola-Rodríguez, M., Neuschitzer, M., Sylla, D., Fairbrother, A., Izquierdo-Roca, V., Pérez-Rodríguez, A., Saucedo, E., 2014. Impact of Sn(S, Se) secondary phases in $C_u2ZnSn(S, S_e)4$ solar cells: a chemical route for their selective removal and absorber surface passivation. ACS Appl. Mater. Interfaces 6 (15), 12744–12751.
Zhang, Y., Liao, C., Zong, K., Wang, H., Liu, J., Jiang, T., Han, J., Liu, G., Cui, L., Ye, Q., Yan, H., Lau, W., 2013. $Cu_2ZnSnSe_4$ thin film solar cells prepared by rapid thermal annealing of co-electroplated Cu–Zn–Sn precursors. Sol. Energy 94, 1–7.